Synthesis of Oxide Nanoparticles by Pulsed Laser Ablation in Liquids Containing a Complexing Molecule: Impact on Size Distributions and Prepared Phases

David Amans, Christophe Malaterre, Mouhamed Diouf, Cédric Mancini, Frédéric Chaput, Gilles Ledoux, G. Breton, Yann Guillin, Christophe Dujardin, Karine Masenelli-Varlot, et al.

Synthesis of Oxide Nanoparticles by Pulsed Laser Ablation in Liquids Containing a Complexing Molecule: Impact on Size Distributions and Prepared Phases

D. Amans,*[,†] C. Malaterre,[†] M. Diouf,[†] C. Mancini,[†] F. Chaput,[†] G. Ledoux,[†] G. Breton,[†] Y. Guillin,[†] C. Dujardin,[†] K. Masenelli-Varlot,[‡] and P. Perriat[‡]

[†]Université de Lyon, Université Lyon 1, UMR CNRS 5620, Laboratoire de Physico-Chimie des Matériaux Luminescents, F-69622 Villeurbanne, France

[‡]Université de Lyon, INSA-Lyon, MATEIS, UMR CNRS 5510, F-69621 Villeurbanne cedex, France

ABSTRACT: We performed laser ablation of doped oxides, Y_2O_3:-$Eu^{3þ}$, Gd_2O_3:$Eu^{3þ}$, and $Y_3Al_5O_{12}$:$Ce^{3þ}$ (YAG:Ce), in an aqueous solution of 2-[2-(2-methoxyethoxy)ethoxy]acetic acid (MEEAA). Nanoparticles are produced and characterized using electron micro-scopy and luminescence spectroscopy. We show that the polyether chain ensures the stabilization of the objects formed in aqueous medium while the complexing group limits their size and sharpens the size distribution. The nanoparticles produced from the sesqui-oxide targets are in a "cubic disordered" phase as expected for very small particles. The ablation of the YAG target leads to a majority of R-Al2O3 and YAG nanoparticles and a minority of YAlO3 nanoparticles. Infrared spectroscopy is used to characterize the nature of the complex formed between the ligand and the particle surface. We demonstrate that the coordination mode of the carboxylate (-COO-) group to metal ions of the nanoparticles' surface is the bridging bidentate mode.

INTRODUCTION

Original optical properties of inorganic nanoparticles are the focus of interest in numerous fields, such as medical imaging and therapeutic,[1−6] microfluidic,[7] nuclear physics (scintillation[8]), or quantum optics.[9] The required optical properties can be up-conversion, scintillation, high luminescence quantum yield, thermoluminescence, photostimulation, or a long coherent lifetime, but the possibility to transfer all these optical properties to the nanoscale is not obvious. To experimentally address this question, pulsed laser ablation in liquids (PLAL) is attractive as a fast screening synthesis method. This versatile bottom-up method allows one quickly synthesize nanoparticles,[10] among which include high-pressure phases (diamond,[10−14] cubic-BN,[15,16] C_3N_4[17]), complex stoichiometries,[18,19] or core−shell nanoparticles (cobalt/carbon,[20] silver/silver oxide,[21] Zn/ZnO[22]). Moreover, gram scale synthesis of pure ceramic nanoparticles has been recently demonstrated.[23] However, during the synthesis of colloidal solutions, the stabilization of small units is a recurring problem. Their aggregations during the target ablation (see the TEM pictures in refs 18 and 24−28) can lead either to coarse particles with broad size distributions or to very unstable precipitates. The use of organic molecules (surfactant molecule, complexing molecules) dissolved in the ablation liquid can solve this problem. In addition to shifting and reducing the size distribution of nanoparticles, these molecules can be used to select a crystallographic phase, to improve the crystallinity, and to functionalize the surface of nanoparticles for future applications. Among the first papers dedicated to PLAL, Mafuné et al.[29] have shown that the nanoparticles' size distribution shifts toward smaller sizes when the surfactant concentration is increased. The authors used an aqueous solution of anionic surfactant, sodium dodecyl sulfate (SDS, or dodecylsulfuric acid sodium), for the silver nanoparticle[29] and gold nanoparticle[30] syntheses. The abundance of silver nanoparticles produced in aqueous solutions of sodium alkyl sulfates, $C_nH_{2n+1}SO_4$−Na (n = 12 corresponds to SDS), has been reported[31] as a function of the hydrocarbon chain length (n). In the case of ZnO, the surfactant is necessary to prevent the hydroxidation of the particles. Indeed, Usui et al.[32] have succeeded in preparing ZnO nanoparticles by laser ablation of a zinc metal plate in a liquid environment using a cationic surfactant (cetyltrimethylammonium bromide, CTAB), an amphoteric surfactant (lauryl dimethylaminoacetic acid betaine, LDA), and a nonionic surfactant (octaethylene glycol monododecyl ether, OGM). CTAB has also been used to synthesize spindle-like GaOOH particles[33] (the spindle-like slowly grow in the solution during a few days after the ablation of a Ga target). SDS has also been used for the preparation of metal oxide-based nanomaterials,[34] such as TiO_2 and SnO_2. Moreover, the nanoparticles' crystallinity and abundance seem to strongly

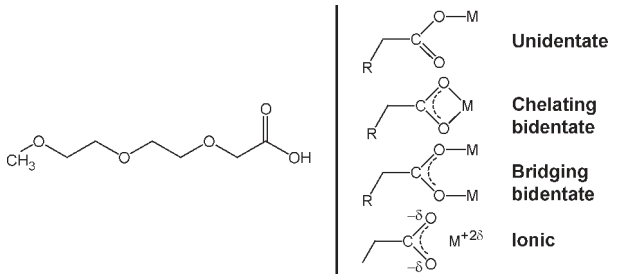

Figure 1. Structure of 2-[2-(2-methoxyethoxy)ethoxy]acetic acid and representative types of coordination of the carboxylate group to the metal ion.

depend on the SDS concentration. Tjuji et al.[35] have performed the preparation of silver nanoparticles in a polyvinylpyrrolidone (PVP) aqueous solution with a two-step process: an ablation, followed by a fragmentation. A solution of PVP dissolved in isopropanol has been previously used to prepare copper nanoparticles.[36] Finally, biocompatible ligands have also been tested[37] for therapeutic applications.

Because of their large gap, doped insulators are particularly suitable as luminescent materials. In this frame, we prepared various doped oxides. We propose to perform the laser ablation in an aqueous solution containing a complexing molecule that fits to surface oxides. The carboxylic acids are well known to react with mineral surfaces through different modes of coordination of the carboxylate ($-COO^-$) group to metal ions. The chemical formula of the selected carboxylic acid MEEAA (2-[2-(2-methoxyethoxy)ethoxy]acetic acid), as well as the coordination modes, is shown in Figure 1. The polyether chain ensures the required stabilization of the objects formed in aqueous medium while the complexing group limits their size. Thus, it is possible to form colloidal solutions whose size distribution of dispersed nanoparticles is narrowed. Unlike the examples mentioned above, the molecule used here contains only hydrophilic groups. MEEAA is used and studied for the first time in PLAL synthesis but has been previously used in an aqueous suspension of zirconia nanoparticles[38,39] and iron oxide nanoparticles.[40] Except for the hydroxidation problem of ZnO,[32] and a model of growth proposed by Mafuné et al.,[29,41] the role of surfactant molecules is still not clearly explained, including how they interact with the different phases of the system during laser ablation.

Infrared spectroscopy is used to characterize the nature of the complex formed between the ligand and the particle surface. There are two bands arising from asymmetric and symmetric stretching vibrations of the COO^- groups at 1630−1580 and 1450−1390 cm^{-1}, respectively, for the analyzed complex. Several studies have shown a correlation between $\Delta\nu_{a-s}$ (frequency separation between the COO^- antisymmetric and symmetric stretches) and the types of coordination of the COO^- group to metal cations.[42−44]

We have synthesized Y_2O_3:Eu^{3+}, Gd_2O_3:Eu^{3+}, and $Y_3Al_5O_{12}$:Ce^{3+} (YAG) nanoparticles by PLAL with the addition of the complexing agent. Rare-earth-doped Gd_2O_3 has been already prepared[26,28] without using complexing molecules. In both studies, the median size was larger than 8 nm. Y_2O_3:Eu^{3+} and Gd_2O_3:Eu^{3+} are well-known red luminescent sesquioxydes. Moreover, gadolinium is a useful contrast agent for nuclear magnetic resonance imaging.[4] Nanoparticles of YAG:Ce are a promising nanoemitter with a short lifetime (<70 ns in bulk[45]), a high quantum yield, and a high stability under irradiation. It is used in white LED, and the nanoparticles are used to develop active tips for near-field scanning optical microscopy.[46] YAG:Ce also shows efficient scintillating properties.[47]

We demonstrate the effect of the MEEAA on the size distribution of the nanoparticles. We then focus our study on Gd_2O_3 nanoparticles. The shift of the size distribution of Gd_2O_3 nanoparticles is investigated as a function of the laser pulse energy. The high atomic number of gadolinium enhances the contrast of TEM pictures by comparison to the yttrium-based nanoparticles. Finally, the luminescence is investigated for different thermal treatments.

EXPERIMENTAL DETAILS

Three targets are used. Targets #C1, #C2, and #C3 correspond, respectively, to monoclinic europium-doped Y_2O_3, europium-doped Gd_2O_3, and cerium-doped YAG. #C2 was a blend of the cubic phase and monoclinic phase. #C1 and #C2 are doped with 5 at. % of europium. They were prepared by standard solid-state reaction techniques from commercial micronic powders. The europium has been added for its luminescence properties. The luminescence of the Eu^{3+} ions is strongly dependent on the symmetry of the crystallographic site and is often used as a structural probe.[48,49] The luminescence spectra give information on the crystallographic phase, the disorder, the crystallinity, and the surface. Depending on the particle sizes, the luminescence intensity is optimal for a europium concentration from 5 to 20 at. %.[50] The lowest values are chosen in order to reduce the perturbation of the crystallinity. #C3 corresponds to cerium-doped YAG with a doping concentration of 2 at. %. #C3 has been prepared by solid-state reaction techniques by A. Petrosyan from the Institute for Physical Research (Ashtarak, Armenia).

The targets were placed at the bottom of a 50 mL beaker and covered by 50 mL of solvent. The solvent is a solution of deionized water containing a complexing molecule, 2-[2-(2-methoxyethoxy) ethoxy]acetic acid (MEEAA) (see Figure 1). The concentration of the complexing molecule was 10^{-2} mol·L^{-1} for the sesquioxides synthesis and 10^{-3} mol·L^{-1} for the YAG synthesis. The measured pHs of the aqueous solution of MEEAA are, respectively, 2.85 and 3.55 (measured $pK_a = 3.8 \pm 0.25$). The pH increases during the laser ablation. The third harmonic YAG laser (λ = 355 nm, Δt = 5 ns, repetition rate = 10 Hz) was focused at the surface of the target. The energy per pulse can be tuned from 2 to 69 mJ·$pulse^{-1}$ by using neutral (density) filters. The irradiation time was between 20 min and 2 h depending on the laser power, in order to keep the solvent clear. It is interesting to note that the complexing molecule, by avoiding the aggregation of the particles, reduces the number of objects larger than the wavelength and thus the Mie diffusion of the laser. Indeed, during the ablation process, some micronic pieces of the target can be torn, dispersed in the solution, and then induce diffusion of the laser pulse. To ensure the stability of the thermodynamic conditions (energy per pulse on the target), the transparency of the solution was particularly controlled. The upper 40 mL of the solutions was collected and centrifuged at 4100 rpm. The centrifugation time was 15 min. For each synthesis, a droplet of the colloidal solution is poured onto 300-mesh copper grids covered with a holey carbon film. The water was then eliminated by natural evaporation. Finally, the whole solution was lyophilized in order to collect powders. Luminescence measurements, infrared absorption, and X-ray diffraction were performed on the powders.

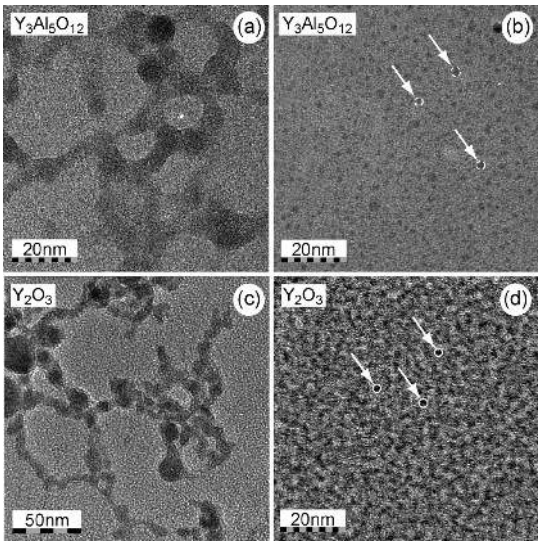

Figure 2. Comparison between the synthesis without the complexing molecule (pictures on the left) and with the complexing molecule (pictures on the right). The TEM pictures (a−d) correspond, respectively, to the syntheses #13, #12, #1, and #2.

Transmission electron microscopy (TEM) images were performed on two apparatus, a JEOL 2010F microscope operating at 200 kV and equipped with energy-dispersive X-ray spectroscopy (EDS) and a TOPCON 002B microscope also operating at 200 kV. The size distribution for each synthesis was deduced from a statistical analysis performed on the transmission electron microscopy pictures. Pictures in Figure 2 are shown as examples. The number of particles referenced for each statistic is, most of the time, higher than 100 (see Table 1). The size distributions are fitted by a log-normal law. The results are reported in Table 1. Fit examples are shown in Figure 3.

The luminescence of the samples was checked from the solution and from the powder in a homemade spectrofluorimeter. The excitation is provided by a 450 W xenon lamp whose discharge is focused at the entrance of a Gemini 180 monochromator from Jobin Yvon. At the exit of the monochromator, the light is refocused on the sample. The luminescence is then collected by an optical fiber and fed into a second monochromator (Triax 320 from Jobin Yvon) and detected by a Peltier-cooled CCD. The excitation spectra were performed with a Peltier-cooled CCD by integrating the luminescence in the appropriate wavelength range. The spectral resolutions of the excitation and emission spectra are given in each scheme.

The Fourier transform infrared spectroscopy (FTIR) was recorded with two pieces of equipment from PerkinElmer. The spectrum GX FT-IR microscope is used when the amount of matter produced is very low. Dry matter is deposited on a silicon substrate and placed in the focal plan of a microscope objective. The spectrometer operates in transmission. The spectral resolution was 4 cm^{-1}. The surface observed was 100 μm × 100 μm. Otherwise, IR spectra were recorded on a PerkinElmer spectrum 100 FTIR with a universal attenuated total reflectance (ATR) sampling accessory. The spectral resolution was 2 cm^{-1}.

To perform X-ray diffraction, the powder is deposited on a microlasso made of nylon, and the measurements are performed on a Gemini S Ultra system from Oxford Diffraction. The X-ray source used has a molybdenum anode (Mo $K\alpha_1$ at 0.07093 nm) focusing the beam on a 300 μm spot.

RESULTS AND DISCUSSION

Characterization of the Nanoparticles. Table 1 shows that the median sizes of the nanoparticles produced using the complexing molecule are between 1.9 and 4.7 nm. For such sizes, the X-ray diffraction spectra are broadened. Following the Scherrer equation,[51−53] a particle of 3 nm leads to a theoretical full width at half-maximum higher than 10% of the diffraction angle (1.8° for a diffraction angle of 15° in 2θ). The combination of the low amount of materials and very small sizes leads to broad-band and noisy spectra, which hinders interpretation. The luminescence spectra and the TEM pictures, correlated with EDS spectra, allow determining the phases and the stoichiometries.

Europium-Doped Sesquioxides. The TEM pictures of Gd_2O_3 are the easiest ones to process. On the Gd_2O_3 samples, roughly 2.5% of the particles show diffraction planes. These diffraction planes correspond to the cubic phase. We have also observed multiple twin boundaries in a few particles. A typical high-resolution image of a Gd_2O_3 particle in a cubic phase is shown in Figure 4. The inter-reticular distances and angles are reported on the image for simplicity reasons but were determined from the electronic diffraction pattern. That does not mean, however, that all the particles are well crystallized or in the cubic phase. Nicolas et al. have synthesized Gd_2O_3:Eu^{3+} by low-energy cluster beam deposition (LECBD) using the same target. They have observed a structural phase transition versus the size[55] with a critical diameter estimated to be 2.8 nm. The particles with a size lower than 2.8 nm are mainly in the monoclinic phase, whereas the larger are mainly in the cubic phase. However, in our case, the complexing agent may relax the Gibbs pressure and then lead to a lower size for the phase transition . The luminescence can also bring much information because the trivalent europium ion is a strong structural probe. The top panel of Figure 5 shows the luminescence spectra of europium-doped Gd_2O_3 in a cubic phase and in a monoclinic phase (from bulk materials). The luminescence of Gd_2O_3:Eu^{3+} prepared by PLAL, and not annealed, is shown in the middle panel of Figure 5. It looks like a mix of the two emissions widened. Such a spectrum resembles those reported in the literature as "cubic disordered" samples.[56] The same behavior is observed on Gd_2O_3 nanoparticles whatever the synthesis methods, including soft chemical routes,[50] LECBD,[55,57] laser pyrolysis,[54] and combustion synthesis.[58] For the smallest particles, the Gibbs pressure induces disorder and maybe an average lattice distortion. The crystallinity is not perfect, and the crystallographic symmetry is slightly different around each europium ion, even if the crystallographic symmetries remain close to the C_2 and S_6 centers in the cubic phase or to the C_s centers in the monoclinic phase. The disorder relaxes the selection rule of the forbidden intraconfigurational f−f dipole transitions and leads to the inhomogeneous broadening observed. Moreover, roughly 30% of the atoms are close to the surface in a nanoparticle of 3 nm. The surface cannot be neglected anymore. In all cases,[50,57,58] an appropriate annealing of the dry powder leads to a well-defined emission of particles in the cubic phase.

Figure 6 shows the luminescence of powder from sample #5 lyophylized. The powder has been deposited on a silicon substrate placed on a THMS600 heating stage from Linkam. The stage is placed in our homemade luminescence measurement setup. The collection of the light is not modified during the whole annealing protocol. The same sample is successively annealed at different temperatures during 15 min. After each annealing, the emission spectrum is collected at room temperature. The

Table 1. Synthesis Parameters and Size Distribution Parameters[a]

synthesis number	target	material	energy per pulse [mJ]	complexing molecule [mol·L^{-1}]	number of particles observed	median size d_0 [nm]	standard deviation [nm]
#1	ref [18]	Y_2O_3	50		124	6.4	2.9
#2	#C1	Y_2O_3	7	10^{-2}	347	1.9	0.35
#3	#C2	Gd_2O_3	2	10^{-2}	57	2.9	0.41
#4	#C2	Gd_2O_3	10	10^{-2}	38	2.8	0.51
#5	#C2	Gd_2O_3	17	10^{-2}	305	2.8	0.62
#6	#C2	Gd_2O_3	26	10^{-2}	170	3.0	0.55
#7	#C2	Gd_2O_3	40	10^{-2}	264	4.1	0.70
#8	#C2	Gd_2O_3	40	10^{-2}	149	3.7	0.75
#9	#C2	Gd_2O_3	55	10^{-2}	231	4.7	1.09
#10	#C2	Gd_2O_3	63	10^{-2}	111	3.08	0.49
#11	#C2	Gd_2O_3	69	10^{-2}	476	4.0	0.89
#12	#C3	$Y_3Al_5O_{12}$	40	10^{-3}	319	2.0	0.31
#13	#C3	$Y_3Al_5O_{12}$	42.5				

[a] The size distributions were fitted with a normalized log-normal law, $[1/(d\sigma(2\pi)^{1/2})]\exp\{-[(\ln(d)-\ln(d_0))^2/(2\sigma^2)]\}$, where d is the particle diameter, d_0 the median diameter, and σ a parameter. The standard deviation is given by $d_0(e^{2\sigma^2}-e^{\sigma^2})^{1/2}$. #1 and #13 correspond to syntheses without complexing molecules. #1 was performed in a previous work.[18]

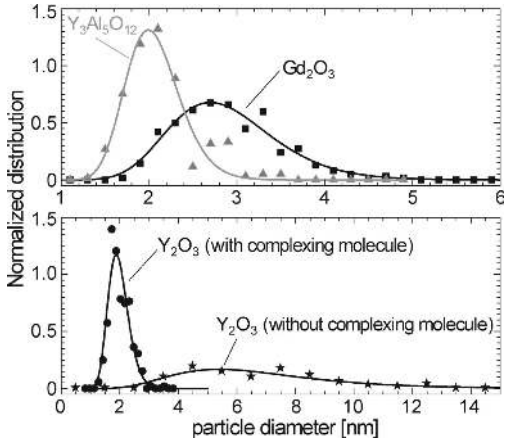

Figure 3. Dots correspond to the particle size distributions deduced from TEM pictures. The lines correspond to the log-normal fit. In the top panel, gray triangles and black squares correspond, respectively, to syntheses #12 (YAG) and #5 (Gd_2O_3). The bottom panel shows the comparison between the synthesis of Y_2O_3 with the complexing molecule (dots, #2) and without the complexing molecule (stars, #1 from our previous work[18]).

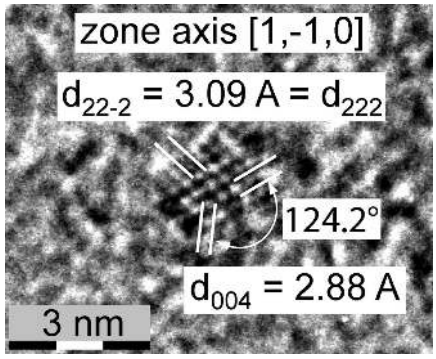

Figure 4. High-resolution picture of a Gd_2O_3 particle in the cubic phase. The particle diameter is 2.2 nm. The measured interplanar distances d_{222} and d_{004} are in good agreement with the theoretical ones (JCPDS file 04-003-4699), respectively, 3.09 ± 0.2 Å for 3.11 Å and 2.88 ± 0.2 Å for 2.69 Å. The measured angle, 124.2 ± 5°, is also in good agreement with the theoretical value of 125.3°.

normalized spectra are shown in Figure 6. For a temperature lower than 470 ± 25 K, the shape of the spectra (not shown) remains identical to the not annealed sample. When the temperature reaches 520 ± 25 K, the broad-band emission is enlarged and progressively splits into two distinguishable bands for a temperature of 670 ± 25 K. At the same time, for a temperature lower than 570 K, the intensity increases. Both observations are explained by the increase of the ratio between the Gd−O bond and the Gd−OH hydroxide, which can be associated with the removal of the water adsorbed on the surface of the nanoparticles. For temperatures between 670 ± 25 K and 810 ± 25 K, we observe the growth of the 611 nm peak. Moreover, for a temperature higher than 570 ± 25 K, the sample becomes brown, which leads to a decrease of the emission intensity. The growth of the 611 nm peak corresponds to the improvement of the nanoparticles' crystallinity. When nanoparticles are not covered by a complexing agent, this improvement is accompanied with a growth of the particles. It has been observed on Gd_2O_3 nanoparticles prepared by LECBD[57] (the growth of the coherent domains size observed by XRD is ascribed to the growth of the particles). In our case, the MEEAA prevents the growth. The tanning of the sample shows that the MEEAA is oxidized, and a carbon shell appears (brown color). At 850 ± 25 K, the MEEAA (and the carbon shell) is completely removed. MEEAA spectral signatures in the FTIR measurement disappear (not shown). The powder on the sample becomes white, and the emission intensity is recovered. This temperature corresponds to the melting point for nanoparticles of about 30 nm,[57] which leads to an instantaneous growth of the particles in the cubic phase. The emission spectrum is then identical to that of the bulk cubic Gd_2O_3:Eu^{3+}.

The Y_2O_3 particle synthesis in the presence of the complexing molecule leads to smaller nanoparticles, down to 3 nm in diameter. No diffraction planes could be observed on the TEM pictures. Nevertheless, the EDS spectrum, shown in Figure 7 and

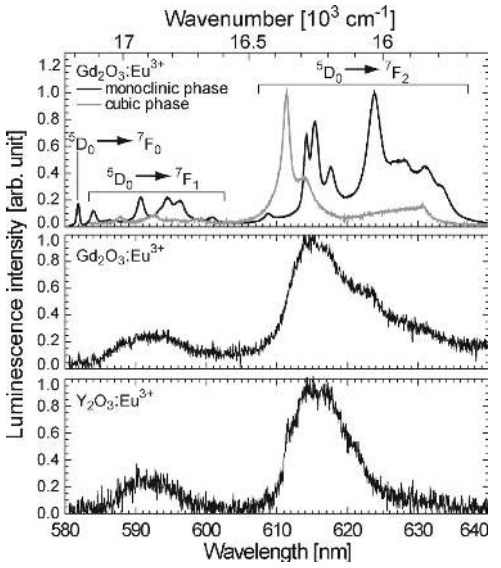

Figure 5. Top panel shows the luminescence spectra of europium-doped Gd_2O_3 in a cubic phase (gray line) and in a monoclinic phase (black line), from bulk samples. The middle panel and the bottom panel show the luminescence from samples synthesized by PLAL and not annealed. Gd_2O_3:Eu^{3+} samples (from #5) are excited at 260 nm. The Y_2O_3:Eu^{3+} (from #2) is excited at 350 nm to preferentially select the nanoparticles [Ledoux et al. (2007)]. The measurement resolution was 0.5 nm.

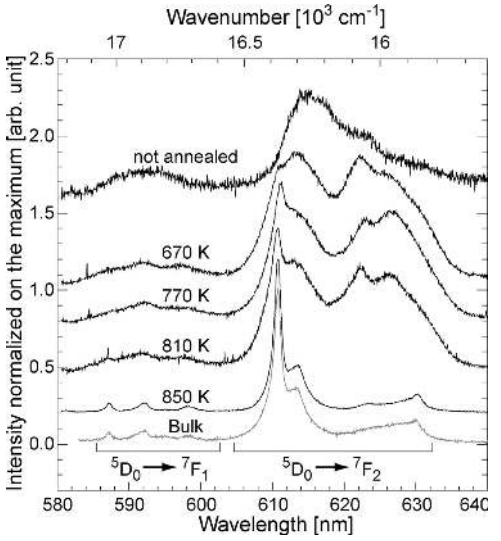

Figure 6. Black curves correspond to the emission of Gd_2O_3:Eu^{3+} powders from #5. The gray curve corresponds to bulk cubic Gd_2O_3:Eu^{3+}. The spectra have been measured at room temperature, after annealing. Each annealing temperature is reported in the scheme. The luminescence was excited in the charge transfer band, at 260 nm. The measurement resolution was 0.5 nm.

performed on the same area than the TEM picture shown in Figure 2d, confirms the presence of yttrium oxide (note that, on the EDS spectrum, the two intense peaks just around 8 and 9 keV can be assigned to copper, arising from the microscopy grid and other microscope pieces). The cubic phase has been observed for the larger nanoparticles in our previous study[18] but can only be supposed in the present one. Indeed, the luminescence spectrum shown in Figure 5 can be ascribed to the "cubic disordered phase"

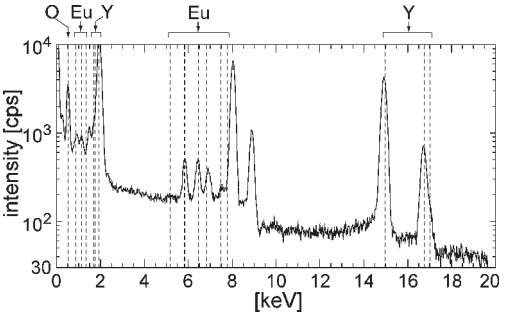

Figure 7. Energy-dispersive X-ray spectrum measured on the TEM picture (Figure 2d) corresponding to the Y_2O_3 synthesis performed using the complexing molecule (#2). The atomic percents are deduced from spectra measured at different positions on the TEM sample. The percentages are 56.5 ± 12.0 at. % of C, 43.3 ± 12.1 at. % of O, 0.18 ± 0.06 at. % of Y, and 0.02 ± 0.01 at. % of Eu.

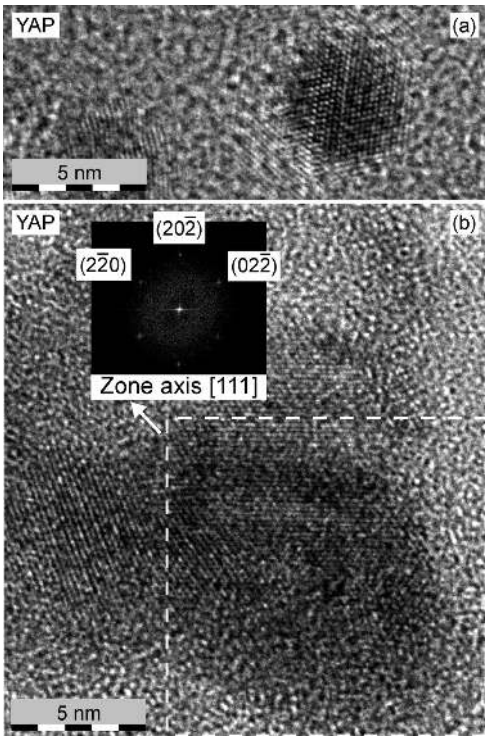

Figure 8. Yttrium aluminum perovskite nanoparticles ($YAlO_3$) 6.3 nm in diameter (panel a) and 10 nm in diameter (panel b). The measured interplanar distances are in good agreement with the theoretical ones (JCPDS file 04-008-4901): d_{2-20} = 2.13 ± 0.03 Å for 2.16 Å, d_{20-2} = 1.83 ± 0.03 Å for 1.86 Å, and d_{02-2} = 2.06 ± 0.03 Å for 2.12 Å. The measured angles 55.0° ± 0.9° between (2−20) and (20−2) and 54.5° ± 0.9° between (20−2) and (02−2) are also in good agreement with the theoretical values, respectively, 55.6° and 54.1°.

and leads to the same discussion than the previous one concerning Gd_2O_3. Moreover, Tissue et al.[59] have observed the cubic phase on annealed particles of Y_2O_3 of 5 nm and a blend of cubic phase and monoclinic phase for larger particles.

Cerium-Doped Yttrium Aluminum Garnet (YAG). The laser ablation of the YAG target in the presence of the complexing molecule also leads to small nanoparticles down to 3 nm in diameter. The associated TEM pictures show a blend of yttrium aluminum perovskite (YAP) nanoparticles (see Figure 8), YAG

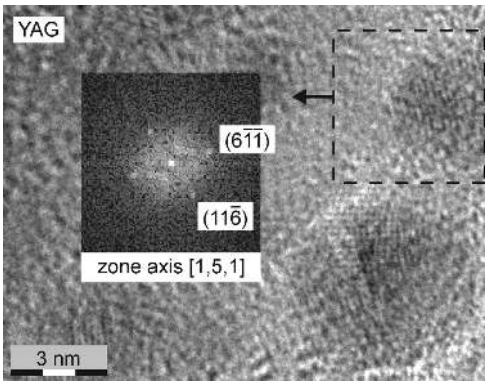

Figure 9. Yttrium aluminum garnet nanoparticle ($Y_3Al_5O_{12}$) 3.4 nm in diameter. The measured interplanar distance d_{11-6} (and d_{6-1-1}) is in good agreement with the theoretical one (JCPDS file 04-001-9940), 1.98 ± 0.09 Å for 1.95 Å. The measured angle, 73.0° ± 2.4°, is also in good agreement with the theoretical value of 73.2°. The atomic ratio Y/Al given by the EDS spectrum is 0.64.

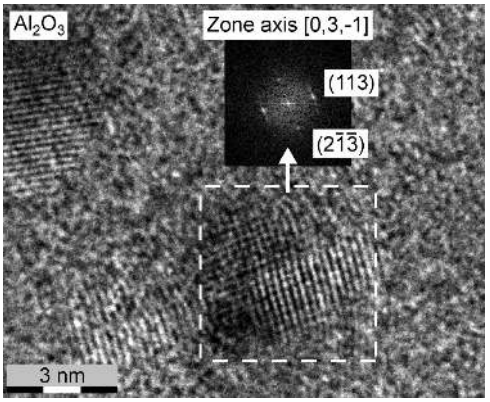

Figure 10. Aluminum oxide nanoparticle (α-Al_2O_3, corundum) 4.7 nm in diameter. The measured interplanar distance d_{113} (and d_{2-1-3}) is in good agreement with the theoretical one (JCPDS file 04-002-3621), 2.09 ± 0.09 Å for 2.09 Å. The measured angle, 83.6° ± 2.4°, is also in good agreement with the theoretical value of 81.3°. The EDS spectrum shows aluminum but not yttrium.

nanoparticles (see Figure 9), and corundum aluminum oxide (α-Al_2O_3) nanoparticles (see Figure 10). Yttrium oxide nanoparticles could not be observed. The corresponding EDS spectra were acquired on large areas containing a lot of nanoparticles, in order to obtain the average composition. Unfortunately, the ratio between the three different stoichiometries cannot be unambiguously determined from the EDS spectra because the main oxygen contribution arises from the complexing molecule and the main carbon contribution arises from the grid. Moreover, the quantification of the oxygen peak is not accurate. Nevertheless, from the Y/Al atomic ratio measured on a large number of particles (Y[at. %]/Al[at. %] = 0.22), several compositions remain possible. One of them could be 19% YAG, 81% alumina, and a negligible amount of YAP. The low amount of YAP is confirmed by luminescence. Indeed, the luminescence can discriminate the YAP:Ce^{3+} and the YAG:Ce^{3+}. Al_2O_3:Ce^{3+} is not known to be an efficient emitter. The interconfigurational 4f−5d transitions of the trivalent cerium ions are very sensitive to the crystal fields due to the large spatial extension of the 5d orbitals. The cerium emission strongly shifts from a host matrix to

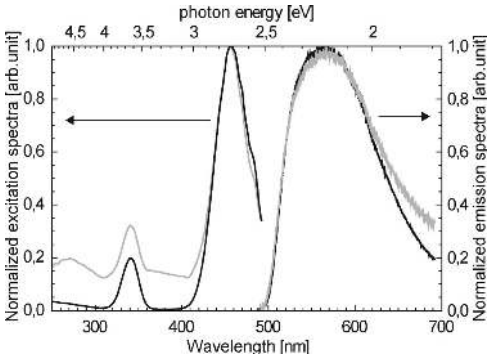

Figure 11. Interconfigurational 4f5d transitions of the trivalent cerium ions in YAG. The excitation spectra and the emission spectra are, respectively, reported in the left and right parts. The spectral resolution of the excitation and emission spectra are, respectively, 4 and 2 nm. The gray curves correspond to the nanoparticles deposited on a silicon substrate (synthesis #12), whereas the black curves correspond to the target #C3. The emission spectra are excited at 480 nm. The excitation spectra correspond to the luminescence integrated between 505 and 620 nm. In each experiment, a 500 nm long-pass filter is put before the detection. The excitation spectra are corrected from the intensity of the light source.

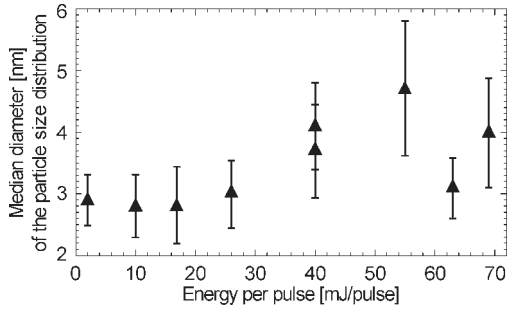

Figure 12. Median diameters of the size distributions of the Gd_2O_3 particles as a function of the energy per pulse (from Table 1). All the syntheses reported are performed using the complexing molecule. The error bars correspond to the standard deviations of the size distributions.

another,[60] up to several hundreds of nanometers. As an example, the maximum of the YAG:Ce^{3+} emission spectrum is around 550 nm, whereas the maximum of the YAP:Ce^{3+} emission spectrum is around 370 nm.[61−63] The emission and excitation spectra of the nanoparticles produced, shown in Figure 11, are almost identical to those performed on a bulk target. The slight broadening can be ascribed to a slight lattice disorder. When the sample is excited in the excitation band of the YAP:Ce^{3+}, above 300 nm,[61−63] the YAP luminescence is not observed. The YAP quantity is then negligible compared with the YAG quantity. We can consider that the nanoparticles produced are mainly α-Al_2O_3 and YAG nanoparticles.

Size Dependence of Pulse Energy. The increase of the median size with the laser energy, reported by several teams,[29,37] is more difficult to observe. Figure 12 does not show any dependence of the particles size deduced from TEM with the laser energy. However, the mean sizes observed by Mafuné et al.,[29] for a comparable range of energy per pulse, are included between 4 and 6 nm with error bars comparable to the size evolution. Our result is somewhat similar. Two experimental biases can explain our behavior. For the lowest energies, the contrast of the smallest

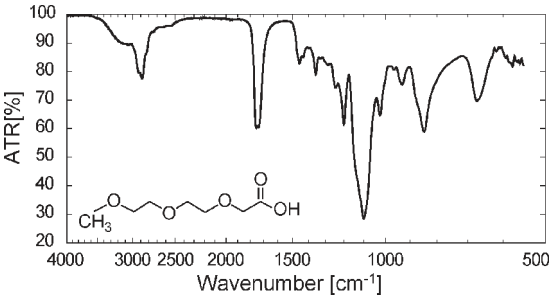

Figure 13. Infrared spectra of MEEAA recorded on a spectrum 100 FTIR with a universal ATR sampling accessory.

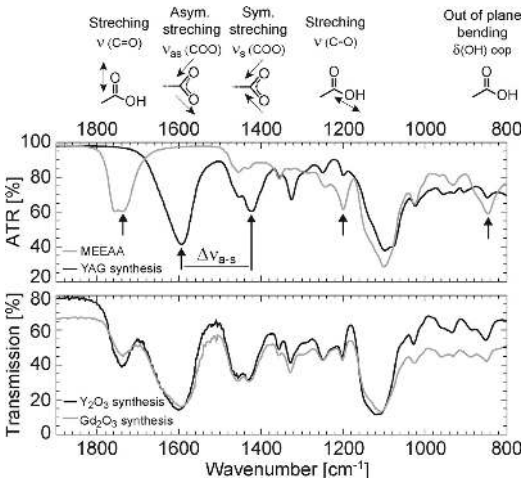

Figure 14. FTIR of MEEAA (top panel, gray curve), MEEAA-capped YAG nanoparticles (top panel, black curve), MEEAA-capped Gd_2O_3 nanoparticles (bottom panel, gray curve), and MEEAA-capped Y_2O_3 nanoparticles (bottom panel, black curve).

particles on the large TEM pictures is limited. The number of particles with a size below 1.5 nm is certainly underestimated. This may lead to a size distribution truncated of the smallest sizes, and this can explain the plateau observed in Figure 12. Concerning the highest energies, the particles produced during a single shot could be bigger than the ones observed on TEM pictures. The ablation is performed in a small volume of liquids, during a time relatively long. The fragmentation of the particles already in the solution is, therefore, possible, even if we took great care to focalize the laser on the target with a wide numerical aperture lens. The fragmentation decreases the size all the more if the laser fluence increases.[64]

Complexing Molecule. For each synthesis performed in an aqueous solution of MEEAA, the aggregation of particles has not been observed compared to the synthesis in deionized water (see Figure 2). Moreover, the addition of a complexing agent in the liquid implies a sharpening of the size distribution, with a ratio between the median size and the standard deviation larger than 4.3 (see Table 1), which becomes comparable with the size distribution obtained with gas pyrolysis[65] (3 for non-size-selected samples and 6−7 for size-selected samples) or low-energy cluster beam deposition techniques. The functionalization of the nanoparticle surface by MEEAA was confirmed by infrared spectroscopy. The FTIR spectrum of 2-[2-(2-methoxyethoxy)ethoxy]-acetic acid (MEEAA) is shown in Figure 13. FTIR spectra of the MEEAA-capped nanoparticles are shown in Figure 14 (centered

Table 2. Infrared Frequencies of 2-[2-(2-Methoxyethoxy)-ethoxy]acetic Acid Observed in Figure 13

sample	wavenumber [cm^{-1}]	assignments
MEEAA	3300−2500	ν(OH)
	2917	$\nu_{as}(CH_2)$
	2876	$\nu_s(CH_2)$
	2819	$\nu(CH)CH_3$
	1740	ν(C═O)
	1454−1429	δ(CH)
	1352	CH_3 umbrella
	1245	ν_{as}(C−C)
	1196	ν(C−O) of −COOH dimer
	1094−1025	ν_{as}(C−O−C)
	931	ν_s(C−C)
	845	δ(OH) out of plane of dimer
	673	CH_2 rock
MEEAA-capped YAG	1593	ν_{as}(COO)
	1423	ν_s(COO)
MEEAA-capped Gd_2O_3	1594	ν_{as}(COO)
	1428	ν_s(COO)
MEEAA-capped Y_2O_3	1600	ν_{as}(COO)
	1431	ν_s(COO)

on the spectral range of interest). FTIR spectra of MEEAA and MEEAA-capped YAG were recorded with the spectrum 100 FTIR with a universal ATR sampling accessory, whereas the spectra of MEEAA-capped Y_2O_3 and Gd_2O_3 nanoparticles were recorded with the spectrum GX FT-IR microscope. The assignment of absorption bands is given in Table 2.

MEEAA exhibits a strong absorption band at 1740 cm^{-1} due to the free carboxylic C═O group. This band disappears in the spectrum of MEEAA-capped YAG nanoparticles, and two new bands appear at 1593 and 1423 cm^{-1}. These bands are assigned to COO^- antisymmetric and symmetric stretching vibrations, respectively. According to Nakamoto,[43] the frequency separation $\Delta\nu_{a-s}$ between ν_{as}(COO) and ν_s(COO) bands can be used as a diagnostic tool to determine the interaction type between the carboxylate head and the metal ions. There are four modes of interaction (see Figure 1): unidentate, chelating bidentate, bridging bidentate, and ionic. It has been shown that a correlation exists between $\Delta\nu_{a-s}$ and the types of coordination of the COO^- groups to metal ions:[42]

$$\Delta\nu_{a-s}(\text{chelating}) < \Delta\nu_{a-s}(\text{bridging}) \sim \Delta\nu_{a-s}(\text{ionic}) < \Delta\nu_{a-s}(\text{unidentate})$$

For a given metal ion, the absorption frequencies ν_{as}(COO) and ν_s(COO) are mainly driven by the O−C−O angle, which differs for each acetate bonding type.[66] The absorption frequencies ν_{as}(COO) and ν_s(COO) have been listed by J. E. Tackett[44] for several metal acetates in aqueous solution and for several solid metal acetates. In this study, the difference $\Delta\nu_{a-s}$ is included between 166 and 170 ± 4 cm^{-1}, indicating that the coordination of carboxylate groups to metal ions is in a bridging bidentate fashion.[40,44] On the spectrum corresponding to the MEEAA-capped YAG nanoparticles, we observe the disappearance of bands at 1740, 1196, and 845 cm^{-1} attributed to ν(C═O), ν(C−O)(−COOH dimer), and δ(OH) (out of plane of dimer), respectively. These three bands do not completely disappear for

the MEEAA-capped sesquioxide because the MEEAA concentration is higher during the synthesis of the sesquioxide nanoparticles. MEEAA molecules remain in excess after the lyophilization of the sesquioxide nanoparticle solutions. The band that appears at 1325 cm^{-1} has not been assigned with certainty; it may correspond to the stretching vibration of the C−C(OO) bond in the complex.

Concerning the YAG synthesis, new experiments should be interesting to improve our understanding of the complexing molecule's role. We must characterize the affinity between the cations, Al^{3+} and Y^{3+}, and MEEAA, to understand the discrepancy between the average stoichiometry measured and the initial target stoichiometry. Moreover, europium-doped YAG will be synthesized to fully characterize the phase produced using europium as a structural probe.

CONCLUSION

We have produced nanoparticles of Y_2O_3, Gd_2O_3, $Y_3Al_5O_{12}$, Al_2O_3, and $YAlO_3$ with average sizes between 2 and 4.5 nm and a narrow size distribution. We have shown that the addition of a complexing agent in the liquid implies a sharpening and a shift of the size distribution, with a ratio between the median size and the standard deviation larger than 4.3. We have demonstrated that the coordination mode of the carboxylate ($-COO^-$) group to metal ions of the nanoparticles surface is the bridging bidentate mode. In the case of the ablation of the YAG target, the influence of MEEAA, on the phase and the stoichiometry of the nanoparticles, is not fully understood yet. Complexing agents seem to act not only on the size distribution but also on the crystallographic phase. It will be interesting to define for each phase an appropriate complexing agent.

AUTHOR INFORMATION

Corresponding Author

*E-mail: david.amans@univ-lyon1.fr.

ACKNOWLEDGMENT

We would like to thank Ashot Petrosyan from the Institute for Physical Research (Armenia) for the synthesis of the YAG target. Research was conducted in the scope of the International Associated Laboratory IRMAS. We would like also to thank R. Vera from the Center for Diffraction Henri Longchambon for invaluable help on the preparation of the samples for XRD. The Centre Lyonnais des Microscopies (CLYM) is thanked for the access to the JEOL 2010F microscope. The CEntre COmmun de Microspectrométrie Optique (CECOMO) is thanked for the access to the PerkinElmer Spectrum GX FT-IR microscope.

REFERENCES

(1) Hahn, A.; Stover, T.; Paasche, G.; Lobler, M.; Sternberg, K.; Rohm, H.; Barcikowski, S. *Adv. Eng. Mater.* **2010**, *12*, B156.

(2) Barcikowski, S.; Hahn, A.; Guggenheim, M.; Reimers, K.; Ostendorf, A. *J. Nanopart. Res.* **2010**, *12*, 1733.

(3) Beaurepaire, E.; Buissette, V.; Sauviat, M. P.; Giaume, D.; Lahlil, K.; Mercuri, A.; Casanova, D.; Huignard, A.; Martin, J. L.; Boilot, T. G. J. P.; Alexandrou, A. *Nano Lett.* **2004**, *4*, 2079.

(4) Bridot, J.-L.; Faure, A.-C.; Laurent, S.; Riviere, C.; Billotey, C.; Hiba, B.; Janier, M.; Josserand, V.; Coll, J.-L.; Vander Elst, L.; Muller, R.; Roux, S.; Perriat, P.; Tillement, O. *J. Am. Chem. Soc.* **2007**, *129*, 5076.

(5) Morgan, N. Y.; Kramer-Marek, G.; Smith, P. D.; Camphausen, K.; Capala, J. *Radiat. Res.* **2009**, *171*, 236.

(6) Casanova, D.; Bouzigues, C.; Nguyen, T.-L.; Ramodiharilafy, R. O.; Bouzhir-Sima, L.; Gacoin, T.; Boilot, J.-P.; Tharaux, P.-L.; Alexandrou, A. *Nat. Nanotechnol.* **2009**, *4*, 581.

(7) Agrawal, A.; Zhang, C. Y.; Byassee, T.; Tripp, R. A.; Nie, S. M. *Anal. Chem.* **2006**, *78*, 1061.

(8) Dujardin, C.; Amans, D.; Belsky, A.; Chaput, F.; Ledoux, G.; Pillonnet, A. *IEEE Trans. Nucl. Sci.* **2010**, *57*, 1348.

(9) Lounis, B.; Orrit, M. *Rep. Prog. Phys.* **2005**, *68*, 1129.

(10) Yang, G. W. *Prog. Mater. Sci.* **2007**, *52*, 648.

(11) Pearce, S. R. J.; Henley, S. J.; Claeyssens, F.; May, P. W.; Hallam, K. R.; Smith, J. A.; Rosser, K. N. *Diamond Relat. Mater.* **2004**, *13*, 661.

(12) Sun, J.; Hu, S. L.; Du, X. W.; Lei, Y. W.; Jiang, L. *Appl. Phys. Lett.* **2006**, *89*, 183115.

(13) Hu, S. L.; Sun, J.; Du, X. W.; Tian, F.; Jiang, L. *Diamond Relat. Mater.* **2008**, *17*, 142.

(14) Amans, D.; Chenus, A.-C.; Ledoux, G.; Dujardin, C.; Reynaud, C.; Sublemontier, O.; Masenelli-Varlot, K.; Guillois, O. *Diamond Relat. Mater.* **2009**, *18*, 177.

(15) Liu, Q. X.; Yang, G. W.; Zhang, J. X. *Chem. Phys. Lett.* **2003**, *373*, 57.

(16) Wang, J. B.; Yang, G. W.; Zhang, C. Y.; Zhong, X. L.; Ren, Z. H. A. *Chem. Phys. Lett.* **2003**, *367*, 10.

(17) Yang, L.; May, P. W.; Yin, L.; Brown, R. *Chem. Mater.* **2006**, *18*, 5058.

(18) Ledoux, G.; Amans, D.; Dujardin, C.; Masenelli-Varlot, K. *Nanotechnology* **2009**, *20*, 445605.

(19) An, W. W.; Miao, J. P.; Zhang, Z. G. *Chem. Phys. Lett.* **2006**, *423*, 386.

(20) Kwong, H. Y.; Wong, M. H.; Leung, C. W.; Wong, Y. W.; Wong, K. H. *J. Appl. Phys.* **2010**, *108*, 034304.

(21) Schinca, D. C.; Scaffardi, L. B.; Videla, F. A.; Torchia, G. A.; Moreno, P.; Roso, L. *J. Phys. D: Appl. Phys.* **2009**, *42*, 215102.

(22) Zeng, H. B.; Cai, W. P.; Hu, J. L.; Duan, G. T.; Liu, P. S.; Li, Y. *Appl. Phys. Lett.* **2006**, *88*, 171910.

(23) Sajti, C. L.; Sattari, R.; Chichkov, B. N.; Barcikowski, S. *J. Phys. Chem. C* **2010**, *114*, 2421.

(24) Tsuji, T.; Hamagami, T.; Kawamura, T.; Yamaki, J.; Tsuji, M. *Appl. Surf. Sci.* **2005**, *243*, 214.

(25) Sasaki, T.; Shimizu, Y.; Koshizaki, N. *J. Photochem. Photobiol., A* **2006**, *182*, 335.

(26) Tarasenko, N. V.; Butsen, A. V.; Nevar, A. A. *Appl. Phys. A: Mater. Sci. Process.* **2008**, *93*, 837.

(27) Ajimsha, R. S.; Anoop, G.; Aravind, A.; Jayarajz, M. K. *Electrochem. Solid-State Lett.* **2008**, *11*, K14.

(28) Singh, S. K.; Kumar, K.; Rai, S. B. *Mater. Sci. Eng., B* **2010**, *166*, 180.

(29) Mafuné, F.; kohno, J.; Takeda, Y.; Kondow, T.; Sawabe, H. *J. Phys. Chem. B* **2000**, *104*, 9111.

(30) Mafuné, F.; kohno, J.; Takeda, Y.; Kondow, T. *J. Phys. Chem. B* **2002**, *106*, 7575.

(31) Mafuné, F.; Kohno, J.; Takeda, Y.; Kondow, T.; Sawabe, H. *J. Phys. Chem. B* **2000**, *104*, 8333.

(32) Usui, H.; Shimizu, Y.; Sasaki, T.; Koshizaki, N. *J. Phys. Chem. B* **2005**, *109*, 120.

(33) Huang, C. C.; Yeh, C. S.; Ho, C. J. *J. Phys. Chem. B* **2004**, *108*, 4940.

(34) Sasaki, T.; Liang, C.; Nichols, W. T.; shimizu, Y.; Koshizaki, N. *Appl. Phys. A: Mater. Sci. Process.* **2004**, *79*, 1489.

(35) Tsuji, T.; Thang, D. H.; Okazaki, Y.; Nakanishi, M.; Tsuboi, Y.; Tsuji, M. *Appl. Surf. Sci.* **2008**, *254*, 5224.

(36) Chandra, M.; Indi, S. S.; Das, P. K. *Chem. Phys. Lett.* **2006**, *422*, 262.

(37) Besner, S.; Kabashin, A. V.; Winnik, F. M.; Meunier, M. *Appl. Phys. A: Mater. Sci. Process.* **2008**, *93*, 955.

(38) Renger, C.; Kuschel, P.; Kristoffersson, A.; Clauss, B.; Oppermann, W.; Sigmund, W. *J. Ceram. Proc. Res.* **2006**, *7*, 106.

(39) Renger, C.; Kuschel, P.; Kristoffersson, A.; Clauss, B.; Oppermann, W.; Sigmund, W. *J. Eur. Ceram. Soc.* **2007**, *27*, 2361.

(40) Déry, J. P.; Borra, E. F.; Ritcey, A. M. *Chem. Mater.* **2008**, *20*, 6420.
(41) Mafune, F.; Kohno, J.; Takeda, Y.; Kondow, T.; Sawabe, H. *J. Phys. Chem. B* **2001**, *105*, 5114.
(42) Nara, M.; Torii, H.; Tasumi, M. *J. Phys. Chem.* **1996**, *100*, 19812.
(43) Nakamoto, K. *Infrared and Raman Spectra of Inorganic and Coordination Compounds*; Wiley: New York, 1986; p 189.
(44) Tackett, J. E. *Appl. Spectrosc.* **1989**, *43*, 483.
(45) Weber, M. J. *Solid State Commun.* **1973**, *12*, 741.
(46) Cuche, A.; Masenelli, B.; Ledoux, G.; Amans, D.; Dujardin, C.; Sonnefraud, Y.; Melinon, P.; Huant, S. *Nanotechnology* **2009**, *20*, 015603.
(47) Ludziejewski, T.; Moszynski, M.; Kapusta, M.; Wolski, D.; Klamra, W.; Moszynska, K. *Nucl. Instrum. Methods Phys. Res., Sect. A* **1997**, *398*, 287.
(48) Chaussedent, S.; Monteil, A.; Ferrari, M.; Del Longo, L. *Philos. Mag. B* **1998**, *77*, 681.
(49) Cormier, G.; Capobianco, J. A.; Morrison, C. A.; Monteil, A. *Phys. Rev. B* **1993**, *48*, 16290.
(50) Flores-Gonzalez, M. A.; Louis, C.; Bazzi, R.; Ledoux, G.; Lebbou, K.; Roux, S.; Perriat, P.; Tillement, O. *Appl. Phys. A: Mater. Sci. Process.* **2005**, *81*, 1385.
(51) Langford, J. I.; Delhez, R.; Dekeijser, T. H.; Mittemeijer, E. J. *Aust. J. Phys.* **1988**, *41*, 173.
(52) Patterson, A. L. *Phys. Rev.* **1939**, *56*, 978.
(53) Scherrer, P. *Gottinger Nachrichten Gesell*. Proceedings of the Royal Society of the Sciences from Goettingen. Weidmannsche Buchhandlung: Berlin, **1918**, p 98.
(54) Ledoux, G.; Leconte, Y.; Amans, D.; Dujardin, C.; Combemale, L.; Herlin-Boime, N.; Reynaud, C. Host size effects on optical properties of Y2O3: Eu3+ and Gd2O3: Eu3+ nanoparticles synthesized by laser pyrolysis. In *Doped Nanopowders: Synthesis, Characterisation, and Applications*; Proceedings of the Symposium on Doped Nanopowders held at the 2006 Fall E-MRS Meeting, Warsaw, Poland, September 4−8, 2006; Trans Tech Publications: Stafa-Zurich, Switzerland, 2007; p 157.
(55) Nicolas, D.; Masenelli, B.; Melinon, P.; Bernstein, E.; Dujardin, C.; Ledoux, G.; Esnouf, C. *J. Chem. Phys.* **2006**, *125*, 171104.
(56) Tissue, B. M. *Chem. Mater.* **1998**, *10*, 2837.
(57) Mercier, B.; Ledoux, G.; Dujardin, C.; Nicolas, D.; Masenelli, B.; Mélinon, P.; Bergeret, G. *J. Chem. Phys.* **2007**, *126*, 044507.
(58) Liu, C.; Liu, J.; Dou, K. *J. Phys. Chem. B* **2006**, *110*, 20277.
(59) Tissue, B. M.; Yuan, H. B. *J. Solid State Chem.* **2003**, *171*, 12.
(60) Dujardin, C.; Gacon, J. C.; Pedrini, C. *Encyclopedia of Materials: Science and Technology*; Elsevier Science: Amsterdam, 2001.
(61) Baryshevsky, V. G.; Korzhik, M. V.; Minkov, B. I.; Smirnova, S. A.; Fyodorov, A. A.; Dorenbos, P.; Vaneijk, C. W. E. *J. Phys.: Condens. Matter* **1993**, *5*, 7893.
(62) Blasse, G.; Grabmaier, B. C. *Luminescent Materials*; Springer-Verlag: Berlin, 1994.
(63) Dunhua, C.; Guangjun, Z.; Jianyu, C.; Qin, D.; Yuchong, D.; Yan, C. *J. Alloys Compd.* **2010**, *489*, 515.
(64) Takami, A.; Kurita, H.; Koda, S. *J. Phys. Chem. B* **1999**, *103*, 1226.
(65) Ledoux, G.; Guillois, O.; Porterat, D.; Reynaud, C.; Huisken, F.; Kohn, B.; Paillard, V. *Phys. Rev. B* **2000**, *62*, 15942.
(66) Deacon, G. D.; Phillips, R. J. *Coord. Chem. Rev.* **1980**, *33*, 227.